



Computational Fluid Dynamics Modelling of a Midlatitude Small Scale upper Ocean Front

P. Cornejo^{1,2†} and H. H. Sepúlveda²

¹ *Mechanical Engineering Department, Faculty of Engineering, University of Concepción, Concepción, Chile*

² *Geophysics Department, Faculty of Physical and Mathematical Sciences, University of Concepción, Concepción, Chile*

Email: pabcornejo@udec.cl

(Received July, 10, 2015; accepted September, 1, 2015)

ABSTRACT

A numerical model is implemented to describe fluid dynamic processes associated with mid-latitude small-scale (10 km) upper ocean fronts by using modified state of the art computational fluid dynamics tools. A periodic system was simulated using three different turbulent closures: 1) URANS-Reynolds Stress Model (RSM, seven equation turbulence model), 2) LES-Standard Smagorinsky (SS, algebraic model), and 3) LES-Modified Smagorinsky, introducing a correction for non-isotropic grids (MS). The results show the front developing instabilities and generating sub-mesoscale structures after four days of simulation. A strongly unstable shear flow is found to be confined within the mixed layer with a high Rossby number ($Ro > 1$) and high vertical velocity zones. The positive (negative) vertical velocity magnitude is found to be approximately $O(10^{-3})$ m/s ($O(10^{-2})$ m/s), one (two) order(s) of magnitude larger than the vertical velocity outside the sub-mesoscale structures, where the magnitude is stable at $O(10^{-4})$ m/s. The latter value is consistent with previous numerical and experimental studies that use coarser grid sizes and therefore do not explicitly calculate the small scale structures. The nonlinear flow introduced by the sub-mesoscale dynamics within the mixed layer and the non-isotropic grid used in the calculations generates a disparity between the predicted horizontal wave-number spectra computed using the RSM model with respect to the linear eddy viscosity model SS. The MS approach improves SS predictions. This improvement is more significant below the mixed layer in the absence of flow nonlinearities. The horizontal spectra predicted with the RSM model fits a slope of -3 for large scale structures and a slope between -2 and $-5/3$ for turbulent structures smaller than 300 m. This work contributes to the investigation of the physical and methodological aspects for the detailed modelling and understanding of small scale structures in ocean turbulence.

Keywords: Submesoscale; Ocean vertical mixing; Turbulence; Geophysical fluid dynamics.

NOMENCLATURE

a	computational grid aspect ratio	T_0	reference temperature
C_p	heat capacity	u_i	i-th velocity component
E	internal energy	$\overline{u'_i u'_j}$	ij-th Reynolds stress component
f	coriolis parameter	V	cell volume
k	thermal conductivity	w	vertical velocity
L_s	mixing length	x_i	i-th cartesian coordinate
p	pressure		
Pr_t	turbulent Prandlt number	α	expansion coefficient
S	source term	δ_{ij}	Kronecker delta
$ \overline{S} $	strain rate magnitud	ϵ	turbulent kinetic energy dissipation rate
S_{ij}	ij-th strain rate tensor component	κ	turbulent kinetic energy
t	time	μ	molecular viscosity
T	temperature	μ_{eff}	effective viscosity

μ_t	turbulent viscosity	τ_{ij}	ij-th stress tensor component
ρ	density	$(\tau_{ij})_{eff}$	ij-th effective stress tensor component
ρ_0	reference density	Ω	angular speed of Earth's rotation

1. INTRODUCTION

The ocean is a dynamic system that involves the interactions of convective phenomena and wave propagation in a wide range of length and time scales. Its energy budget is provided by atmospheric forcing from wind, heat and salinity flows. This energy budget is mostly provided by large scale turbulent structures (gyres) that are confined by bathymetry and shorelines and that have a length scale of $O(1)$ km. The shear of these gyres or oceanic currents distorts the flow pattern, making the waves that propagate through them grow unstably. This phenomenon corresponds to barotropic (horizontal shear) and baroclinic (vertical shear) instabilities, and both are first order processes in the energy transfer from large scale to mesoscale turbulent structures, with length scales reaching $O(10 - 100)$ km, and are in thermal wind balance, i.e., horizontally in geostrophic balance and vertically in hydrostatic balance. In low latitudes, mesoscale structures are described by geostrophic dynamics (Rhines 1979), developing an inverse energy cascade (Boffetta *et al.* 2000), where the smaller scale structures transfer their energy to larger scales, increasing their size. This process is repeated until a characteristic scale length, known as the Rhines scale, is reached. From this point, the turbulent structures stop growing and begin a process of progressive deformation where the mesoscale vortices are transformed into Rossby wave packages, which are dispersed at the coast (Rhines 2006). In mid-latitudes, the mesoscale structures are described by quasi-geostrophic dynamics (Charney 1971), where ageostrophic processes begin to play an important role. This feature of the geostrophic ocean has motivated the identification of the alternative energy dissipation pathways (besides boundary layers) of the mesoscale structures. Particularly, it has motivated the study of surface frontal systems, where it has been found that dissipation is enhanced (Charney 2011). In mid-latitudes, these fronts generate sub-mesoscale ($O(1)$ km) turbulent structures, which develop a direct energy cascade Martin and Richards (2008), Boccaletti *et al.* (2007), Skillingstad and Samelson (2008), Martin and Richards (2001), Mahadevan *et al.* (2010), thus transferring their energy to the turbulent 3D structures (Van Roekel *et al.* 2012; Skillingstad and Samelson 2012) through processes related to stratified turbu-

lence, Kelvin-Helmholz instabilities, Langmuir turbulence, and so on (Martin and Richards 2008; Skillingstad and Samelson 2008). These 3D structures, in turn, follow classic Kolmogorov turbulence behavior and their energy is finally dissipated as heat (Jiménez 2010). Mesoscale structures are hotspots of primary productivity and maintain high vertical velocities in their cores. Their inner temperature is different from the temperature of the surrounding waters, deforming the density field on its periphery and generating a front with vertical isopycnals. This fact perturbs the flow in thermal wind balance and creates ageostrophic circulation as a reaction to the disturbance of the balance to maintain it (Skillingstad and Samelson 2008). In mid-latitudes this process (frontogenesis) evolves unstably, creating areas with intense local dynamics depending less on the Earth rotation ($Ro \approx 1$), thus promoting the formation of turbulent sub-mesoscale structures through unbalanced ageostrophic baroclinic instabilities (Lapyer *et al.* 2006; Molemaker and McWilliams 2005; Mahadevan *et al.* 2010; Capet *et al.* 2008; Klein *et al.* 2011), as well as symmetrical instabilities (Thomas *et al.* 2013). Previous work has reported vertical velocities associated with sub-mesoscale structures with $O(10^{-4})$ m/s, both in numerical (Mahadevan *et al.* 1996; Skillingstad and Samelson 2008; Capet *et al.* 2008) and experimental studies (Flament *et al.* 1985; Paduan and Niiler 1990; Dewey *et al.* 1991; Pollard and Regier 1992). These are typically one order of magnitude higher than vertical velocities associated with mesoscale structures (Skillingstad and Samelson 2008; Mahadevan *et al.* 1996; Ali, Nazar, Arifin, and Pop 2009; Wunsch and Raffaele 2004), which has direct influence on primary productivity, mixed layer stratification and therefore, on climate. Several theories predict the shape of the horizontal velocity wavenumber spectrum for different regimes of ocean turbulence. The interior quasi-geostrophic theory of Charney (1971) predicts a spectrum with a slope of -3 for the inertial range in an interior geostrophic scenario away from the surface and where only the anomalies of potential vorticity are important, neglecting density anomalies. On the other hand, the surface quasi-geostrophic theory of Blumen (1978) considers a situation where the flow is attributable to surface density anomalies and where the internal

potential vorticity remains constant, predicting a wave-number spectrum with a slope of -2 for the submesoscale inertial range. Finally, Boyd (1992) showed that by including ageostrophic processes in the surface quasi-geostrophic theory of Blumen (1978), the slope of the spectrum is adjusted, reaching $-5/3$ in the inertial range of the submesoscale. A detailed discussion on the predictions of the above mentioned theories and their implications can be found in Callies and Ferrari (2013). Due to the limitations of observational tools, the formation and dynamics of the submesoscale structures has been described, in general, by using numerical simulation tools (Özgökmen *et al.* 2011; Özgökmen and Fischer 2012; Capet *et al.* 2008; Mahadevan *et al.* 1996; Klein *et al.* 2010). Studies that adopt modelling strategies inherited from the regional oceanographic modelling describe turbulent subgrid-scale structures with moderately complex parameterizations. Commonly, these models use computational grids with a horizontal resolution two orders of magnitude larger than the vertical resolution as a result of the high aspect ratio of the turbulent structures to be described and the magnitude of the horizontal ($O(10^{-1})$ m/s) and vertical ($O(10^{-4} - 10^{-5})$ m/s) velocities involved. Due to this set up, regional oceanographic models usually separate horizontal and vertical turbulence diffusions. However, this approximation prevents the energy transfer between the horizontal and vertical turbulent velocity fluctuations from being parameterized. In some cases, the horizontal diffusion is not included due to the numerical diffusion inherent to the discretization schemes employed. In other cases, it is described by using a constant diffusion coefficient. The vertical turbulent diffusion is commonly modeled by using a constant diffusion coefficient, considering diffusion coefficients depending on the vertical coordinate (Ramachandran *et al.* 2013) or, in some cases, algebraic models, such as the Smagorinsky model (Mahadevan *et al.* 1996). Models based on computational fluid dynamics (CFD) are used in a number of engineering applications. However, in geophysics, their application is less broad due to the capacity of current computers, which restricts them to small scale problems. Their use in engineering applications with highly curved flow lines has led to the development and implementation of high performance turbulence models. This is the case for the turbulence model based on the independent description of each component of the Reynolds stress tensor or second moments. The proliferation of the use of this model in engineering applications is still limited by the

complexity of the implementation and interpretation of the underlying physics as well as the associated computational cost, even when it has a better performance compared to linear eddy viscosity models in problems involving nonlinear velocity fields and therefore in conditions of non-isotropic turbulence (Flament *et al.* 2011; Launder *et al.* 2006). The aim of the present manuscript is to study a small scale (10 km) upper mid-latitude frontal system, with emphasis on the vertical velocity field, spectral energy distribution of horizontal structures and their relation to the formation of sub-mesoscale structures. For this, we use linear and nonlinear approximations to model subgrid-scale turbulent structures and a high-resolution computational grid ($dx=dy=30$ m, $dz < 10$ m inside the mixed layer). The model was implemented in the commercial CFD code ANSYS-FLUENT, including trivial modifications in the conservation equations to consider the effects of the Earth's rotation and water column stratification. We compare three different approaches to describe the turbulent subgrid-scale structures: the Reynolds Stress Model, which calculates the components of the Reynolds stress tensor by means of the solution of an additional conservation equation for each component (Flament *et al.* 2011; Launder *et al.* 2006); the standard Smagorinsky model (Smagorinsky 1963); and the Smagorinsky model, including a modification in the estimation of the turbulent viscosity to use non-isotropic grids according to Rhines (1993). The numerical results obtained are compared with theoretical predictions and data from previous numerical and experimental studies available in the literature.

2. MATHEMATICAL MODEL

2.1 Hydrodynamics

The unforced evolution of a surface ocean front is a fluid dynamics problem of gravitational balance modified by planetary rotation. The system hydrodynamics is described by the joint solution of the continuity, momentum and energy conservation equations. The following equation describes the mass conservation for an incompressible fluid:

$$\frac{\partial \rho}{\partial t} + \frac{\partial}{\partial x_i}(\rho u_i) = 0 \quad (1)$$

Momentum conservation is described by means of the following transport equation:

$$\frac{\partial}{\partial t}(\rho u_i) + \frac{\partial}{\partial x_j}(\rho u_i u_j) = \frac{\partial p}{\partial x_i} + \frac{\partial \tau_{ij}}{\partial x_j} + \frac{\partial}{\partial x_j}(-\rho \overline{u'_i u'_j}) + S \quad (2)$$

where ρ is the fluid density; u_i and x_i are the i -th ($i=3$) component of velocity and coordinate,

respectively; p is the pressure; and τ_{ij} is the stress tensor, which is described by the following equation:

$$(\tau_{ij})_{\text{eff}} = \mu_{\text{eff}} \left(\frac{\partial u_j}{\partial x_i} + \frac{\partial u_i}{\partial x_j} \right) - \frac{2}{3} \mu_{\text{eff}} \frac{\partial u_k}{\partial x_k} \delta_{ij} \quad (3)$$

where $\mu_{\text{eff}} = \mu + \mu_t$ is the effective viscosity considering molecular and turbulent properties of fluid and flow respectively, $-\rho \overline{u'_i u'_j}$ is the Reynolds stress tensor resulting from the averaging process of the Navier-Stokes equations that must be properly modeled, and $S = [fv - f_* w, -fu, f_* u]$ is the source term that incorporates the Coriolis effect, where the Coriolis coefficients are calculated as $f = 2\Omega \sin(\phi)$ and $f_* = 2\Omega \cos(\phi)$ with $\Omega = 7.2921 \times 10^{-5}$ rad/s, the angular speed of Earth's rotation. Energy conservation is described with the following transport equation:

$$\frac{\partial}{\partial t} (\rho E) + \frac{\partial}{\partial x_i} [u_i (\rho E + p)] = \quad (4)$$

$$\frac{\partial}{\partial x_j} \left[\left(k + \frac{c_p \mu_t}{Pr_t} \right) \frac{\partial T}{\partial x_j} + u_i (\tau_{ij})_{\text{eff}} \right]$$

where $E = h + \frac{v^2}{2} - \frac{p}{\rho}$ denotes total energy, k is the thermal conductivity, c_p is the caloric capacity, Pr_t is the turbulent Prandtl number and μ is the turbulent viscosity that is estimated to be $\mu_t = C_\mu \kappa^2 / \varepsilon$ in the case of the RSM approach and determined directly in the case of the Smagorinsky model, with κ as the turbulent kinetic energy and ε as the turbulent kinetic energy dissipation rate. The dissipation term that involves the deviatoric stress tensors $(\tau_{ij})_{\text{eff}}$ shown in Eq.(3) describes the thermal energy created by the predominance of viscous stresses on the inertial effects at the dissipation scale. Seawater density is usually estimated using an equation of state that depends on salinity, pressure, and temperature. For simplicity, in this study, we consider only density as a function of temperature, as shown by the following equation:

$$\rho = \rho_0 [1 - \alpha(T - T_0)] \quad (5)$$

where $\rho_0 = 1028 \text{ kg/m}^3$ and $T_0 = 283 \text{ K}$ are reference values and $\alpha = 1.7 \times 10^{-4} \text{ K}^{-1}$ is the thermal expansion coefficient. The above equations describing the system hydrodynamics must be closed with a turbulence model, which must account for the components of the Reynolds stress tensor $-\rho \overline{u'_i u'_j}$ that result from the averaging process. In this manuscript, turbulence is an important aspect, so it is described in detail in the next section.

2.2 Turbulence Modelling

Turbulent flows are characterized as those presenting a wide spatial and temporal variability.

They are highly unstable, nonlinear and efficient in mixing themselves and the properties that they transport (energy, salinity, chemical species, etc.) due to macroscopic fluctuations of the fluid particles. Its spectrum is composed of a part associated with larger length scale structures (low wave-number) that mainly depend on the geometry and boundary conditions and contain most of the energy, and in real problems, there is no analytical model that can describe them. Therefore, in the field of numerical modelling they must be calculated explicitly. The second part of the spectrum is associated with the smaller length scale structures (high wave-number or subgrid-scales), which, due to computational cost constraints, cannot be directly calculated and their effect on the mean flow must be modeled. Based on numerical simulation, the issues raised by the turbulent characteristic of fluid flows are reduced to the problem of how these sub-grid structures $-\rho \overline{u'_i u'_j}$ are modeled. There are several turbulence models with different complexities and properties. It is possible to differentiate two major modelling approaches. The first is based on the Boussinesq hypothesis

$$-\rho \overline{u'_i u'_j} = \mu_t \left(\frac{\partial u_i}{\partial x_j} + \frac{\partial u_j}{\partial x_i} \right) - \frac{2}{3} \left(\rho \kappa + \mu_t \frac{\partial u_k}{\partial x_k} \right) \delta_{ij} \quad (6)$$

where the Reynolds stress tensor components are described using a linear function, the strain rate multiplied by a turbulent viscosity, which leads to the closure problem regarding how this turbulent viscosity is estimated. This approach assumes an isotropic turbulence condition and therefore the turbulence models based on it behave well in linear flows or flows with low curvature. Models based on this approach range from zero equation models or models where the turbulent viscosity is calculated through an algebraic equation commonly based on the mixing length, such as the Smagorinsky model (Smagorinsky 1963); one equation models (Allmaras and Spalart 1992); two equation models, like the $\kappa - \varepsilon$ or $\kappa - \omega$ model, and finally models of three or four equations, such as the transition $\nu 2f$ model or the potential turbulence model of Perot (1999). On the other hand, a second modelling approach is based on the independent description of each component of the Reynolds stress tensor by solving the conservation equation Eq.(11). This model has a larger associated computational cost and underlying physics complexity. However, it is well behaved and more accurate in nonlinear flow fields or in problems that involve highly curved flow lines and that deviate from the isotropic turbulence condition. Both modelling approaches are described in the following subsections.

Algebraic closure: Smagorinsky Model

The Smagorinsky model (Smagorinsky 1963) is a turbulence model that is widely used in geophysics and engineering. This model uses the Boussinesq hypothesis for the calculation of the subgrid-scale stresses in terms of the mean flow velocity field. Turbulent viscosity is estimated by using the following algebraic equation

$$\mu_t = \rho L_s^2 |\bar{S}| \tag{7}$$

where the subgrid strain-rate magnitude $|\bar{S}| = \sqrt{2\bar{S}_{ij}\bar{S}_{ij}}$ is estimated through the strain rate defined by

$$\bar{S}_{ij} \equiv \frac{1}{2} \left(\frac{\partial \bar{u}_i}{\partial x_j} + \frac{\partial \bar{u}_j}{\partial x_i} \right) \tag{8}$$

where L_s is the mixing length. In computational grids with similar resolutions in all three directions, the mixing length is estimated using $L_s = \min(\kappa d, C_s V^{1/3})$, where κ is the Von Karman constant, d is the closest distance to the wall, $C_s = 0.11$ is a model constant estimated for the first time by Lilly (1967) for homogeneous isotropic turbulence, and V is the computational cell volume. Therefore, when using a nearly isotropic grid, the estimation of the mixing length is adequate because the cubic root of the cell volume is similar to the size of the elements used in the discretization. However, in non-isotropic grids or grids with larger aspect ratios, an error is introduced by estimating the mixing length as the cubic root of the cell volume and, in this case, does not represent the computational grid resolution in either direction. Thus, in grids with high and moderate aspect ratios, a modification must be introduced to correct this problem. For this, following the work of Rhines (1993), the standard Smagorinsky model is modified to correct the mixing length estimation using the following equation

$$L_s = V^{1/3} f(a_1, a_2) \tag{9}$$

where $f(a_1, a_2)$ is a function that modifies the mixing length calculation of the standard model, which is defined by using energy balance considerations in isotropic turbulence according to

$$f(a_1, a_2) = 1 + \frac{2}{27} [\ln(a_1)^2 - \ln(a_1)\ln(a_2) + \ln(a_2)^2] \tag{10}$$

with $a_1 = \Delta x/\Delta z$ and $a_2 = \Delta y/\Delta z$, where Δx and Δy are the horizontal resolutions and Δz is the vertical resolution of the computational grid.

Second moment closure: Reynolds Stress Model (RSM)

The linear eddy viscosity models based on the Boussinesq hypothesis are known to have a mod-

erate accuracy in problems involving stagnation areas, highly curved flow lines, and in general, flows with more than one significant component of the mean velocity gradient, because they poorly represent the turbulent energy levels in conditions departing from isotropic turbulence. Abandoning the Boussinesq hypothesis, the RSM model closes the Reynolds Averaged Navier-Stokes equations (Eq.(2)) by solving an additional conservation equation for each component of the Reynolds stress tensor. The exact form of this equation is derived based on the momentum conservation equation for the velocity fluctuations u'_i that is obtained by subtracting the averaged equation (Eq.(2)) from the instantaneous velocity equation (the exact equation before averaging). Then by multiplying u'_i times u'_j , both derived in the same way, and averaging, the equation describing the conservation of $-\rho \overline{u'_i u'_j}$ is obtained

$$\begin{aligned} \frac{\partial}{\partial t} (\rho \overline{u'_i u'_j}) + \frac{\partial}{\partial x_k} (\rho u_k \overline{u'_i u'_j}) = & \left[\overline{u'_j u'_k} \frac{\partial u_i}{\partial x_k} + \overline{u'_i u'_k} \frac{\partial u_j}{\partial x_k} \right] \tag{11} \\ & - 2\mu \overline{\frac{\partial u'_i}{\partial x_k} \frac{\partial u'_j}{\partial x_k}} + p' \left(\frac{\partial u'_i}{\partial x_j} + \frac{\partial u'_j}{\partial x_i} \right) \\ & - \frac{\partial}{\partial x_k} \left[\overline{u'_i u'_j u'_k} - \mu \overline{\frac{\partial u'_i u'_j}{\partial x_k}} + p' (\delta_{jk} u_i + \delta_{ik} u_j) \right] \\ & - \rho \beta (g_i \overline{u'_j \theta} + g_j \overline{u'_i \theta}) \end{aligned}$$

where the first and second term of the left side of Eq.(11) describe the total change of the ij -th component of the Reynolds stress tensor (RSTC), which originates from imbalance in the right side terms. The five terms of the right side of the Eq.(11) represent, from left to right: the stress production due to the strain rate of the mean velocity field; the stress dissipation; the pressure strain term; the stress diffusion due to molecular effects, turbulent velocity fluctuations and pressure fluctuations; and the stress production due to buoyancy effects. Note that the pressure strain term does not contribute to modification of the turbulent energy level in incompressible flows but acts to redistribute the turbulent kinetic energy among the normal components of the stress tensor. Terms associated with total change, molecular diffusion and stress production due to mean flow strain rate do not require any modelling. In fact, one of the advantages of Eq.(11) is that the form of the stress production term independently weights the mean velocity gradients and therefore does not assume isotropic turbulence conditions, allowing a more accurate description of nonlinear fluid flows. However, the stress production terms due to buoyancy effects, turbulent diffusion, dissipation and the pressure strain term must be modeled to close the system. The Reynolds Stress Model is available

in the ANSYS-FLUENT code. The description of how each term in Eq.(11) is modeled is very extensive and is beyond the scope of this study. However, it can be found in Launder *et al.* (2006) and Flament *et al.* (2011).

3. COMPUTATIONAL MODEL

In this article, we seek to describe the formation and dynamics of sub-mesoscale turbulent structures as a result of the unforced evolution of an upper ocean front formed by a mesoscale strain field. With this objective, the periodic model shown in the Fig. 1. was implemented. It extends 10 km across the front (N-S) and 5 km in the periodic along the front direction (W-E). Depth has a constant value of 500 m. Front fields were initialized by considering a 50 m deep mixed layer. The density variation in the N-S direction is considered according to $(\Delta\rho/2)(1 - \exp(Y/2))/(1 + \exp(Y/2))$, with $\Delta\rho = 0.1 \text{ kg/m}^3$, where Y represents the horizontal coordinate in the N-S direction (Fig. 1.b). Under the mixed layer, density variation is considered until a depth of 250 m, and between 50 and 250 m, the depth is initialized as weakly increasing, following $(\Delta\rho)/2(1 - \exp(Y/2))/(1 + \exp(Y/2))$, where $\Delta\rho = 0.1(250 + Z)/200 \text{ kg/m}^3$ with Z as the vertical coordinate (positive upwards). Below 250 m depth, the density field is constant in the N-S direction. Fig. 2. shows a vertical view of the initial density field. The velocity field is initialized with a baroclinic jet in thermal wind balance according to the following equation:

$$u = -\frac{1}{f} \frac{\partial p}{\partial y} \quad (12)$$

where u is the velocity in the along front direction in m/s and the pressure p is estimated using the hydrostatic balance $p = -\rho gz$. Fig. 1.a and Fig. 1.b present the initial velocity and den-

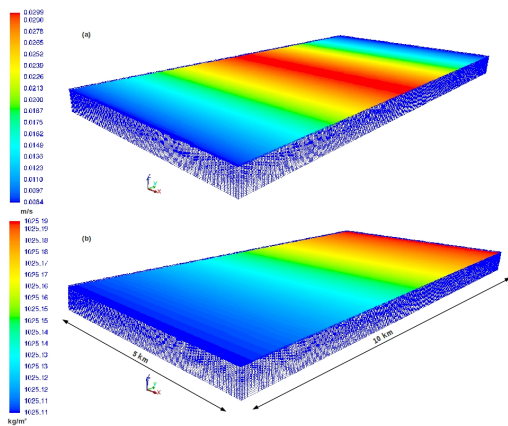


Fig. 1. Computational model: mesh and initial conditions (a) velocity and (b) density fields at surface.

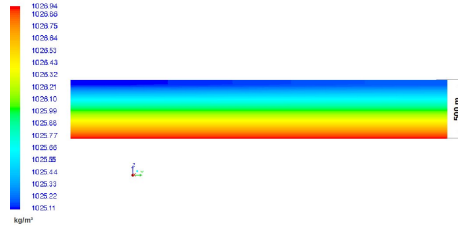


Fig. 2. Vertical density field across the front.

sity fields at the surface. The Coriolis parameter was considered to be 10^{-4} , associated with mid-latitudes. The control volume was discretized with a low aspect ratio hexahedral grid of $2.2e6$ cells, a horizontal uniform grid resolution of 30 m and a stretched vertical grid using a uniform element size of less than 10 m in the first 100 m, varying to a vertical grid resolution of 30 m at 500 m. Each time step is considered 120 s. Under these conditions the estimated Stone fastest-growing rate length scale and growth time reach 3 km and 1 day, and both are consistent with domain dimensions, grid resolution and time step. Boundary conditions are selected to implement a periodic channel; the domain boundaries in the across front direction were described as periodic, and both boundaries in the along front direction as well as the domain lid and bottom were described as walls without considering the viscous effects. Second order discretization schemes are used to solve all of the equations. For pressure-velocity coupling, the SIMPLE (semi-implicit method for pressure-linked equations) scheme is used. The same configuration is used in all of the simulations in the three modelling approaches: RSM, SS and MS. The model described above was implemented in the commercial CFD code ANSYS-FLUENT 14.0, introducing modifications to the conservation equation through User Defined Functions (UDF) to include the effects of Earth's rotation and water column stratification to describe geophysical fluid dynamic problems. The Standard Smagorinsky subgrid-scale model existing in ANSYS-FLUENT was also modified through UDF to correct the estimation of turbulent viscosity when using non-isotropic computational grids.

4. RESULTS

The model was run for 6 days for each of the three modelling approaches: RSM, MS and SS. The results show the front developing instabilities within the mixed layer after the second day of model initialization. These instabilities become increasingly large in amplitude, result-

ing in the emergence of coherent sub-mesoscale structures on the fourth day of simulation. The results shown below correspond to the fifth day after the front was initialized. We present snapshots of different flow variables within and below the mixed layer to assess small-scale ocean turbulent flow features and compare the performance of linear and nonlinear turbulence models. Fig. 3. and Fig. 4. present the density distribution and horizontal velocity field at a 25 m depth inside the mixed layer. It is possible to observe the appearance of coherent turbulent structures that generate a nonlinear flow condition inside the mixed layer. In contrast, a low curvature linear flow is observed below the mixed layer (Fig. 5). Fig. 6. presents a 3D view of the mixed layer sub-mesoscale vortex through an iso-surface of $Ro = 1$. The dy-

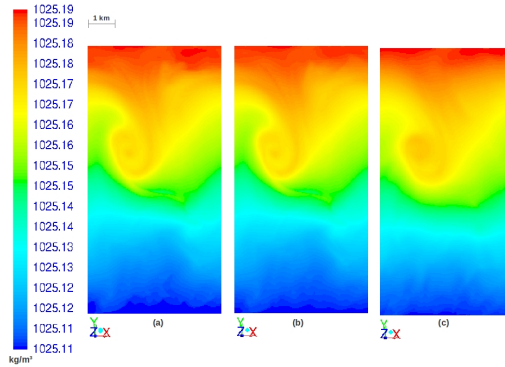


Fig. 3. Density field at 25 m depth: (a) RSM, (b) MS and (c) SS.

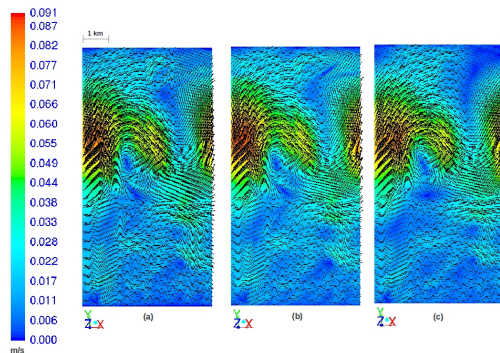


Fig. 4. Horizontal velocity field at 25 m depth: (a) RSM, (b) MS and (c) SS.

namics of the sub-mesoscale structures depend on Earth’s rotation and local processes. This dependency is assessed by the Rossby number, which is a ratio between relative and planetary vorticity. Fig. 9. and Fig. 10. show the Rossby number distribution within and below the mixed

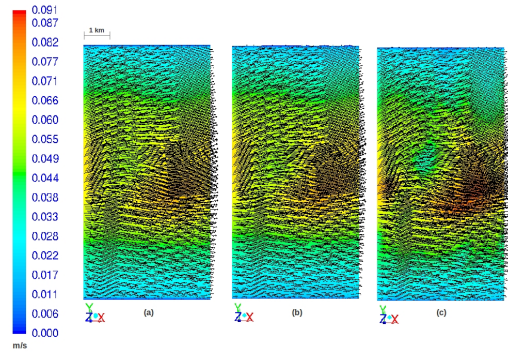


Fig. 5. Horizontal velocity field at 75 m depth: (a) RSM, (b) MS and (c) SS.

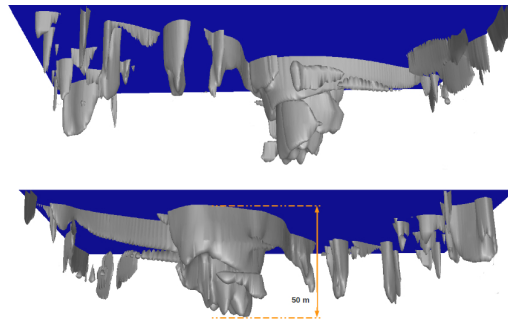


Fig. 6. 3D view of submesoscale eddy.

layer. Within the mixed layer, the Rossby number distribution shows high sub-mesoscale activity, developing filaments of $Ro \approx 1$ and areas with ($Ro > 1$) that have locations that are correlated with the high vertical velocity zones shown in Fig. 7. The vertical velocity magnitude in such areas scales with the prediction of the surface quasi-geostrophic theory from Ali *et al.* (2009) $w = Ro^2 B^{-1} H f_0 = 0.0061$ m/s, where $Ro = 1.1$ (from Fig. 9), $H = 50$ m, $f_0 = 10^{-4}$ and the Burger number B is equal to 1. This condition ($B=1$) can be checked in several ways. Following Skillingstad and Samelson (2008), we checked the scaling between the sub-mesoscale aspect ratio $= HL = 501500 = 0.03$, with L as the horizontal length scale (Fig. 4), H as the mixed layer depth, and the ratio $fN = 0,00010,0023 = 0,04$, where N is buoyancy frequency. Within and below the mixed layer, the MS and RSM modelling approaches predicted similar flow characteristics. In contrast, the SS modelling approach predicted different flow characteristics in terms of the Rossby number distribution: Fig. 9.c and Fig. 10.c, horizontal velocity: Fig. 4.c and Fig. 5.c and vertical velocity field: Fig. 7.c and Fig. 8.c. Fig. 13. and Fig. 12. show plots of the wave-number spectra computed using transects

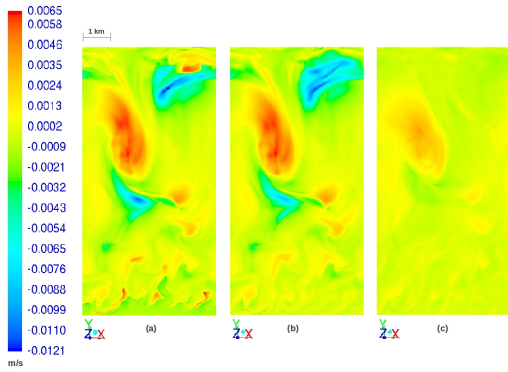


Fig. 7. Vertical velocity field at 25 m depth: (a) RSM, (b) MS and (c) SS.

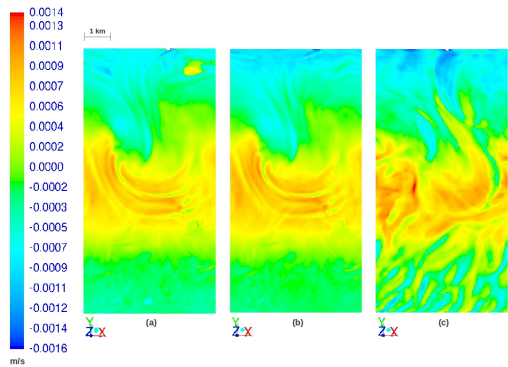


Fig. 8. Vertical velocity field at 75 m depth: (a) RSM, (b) MS and (c) SS.

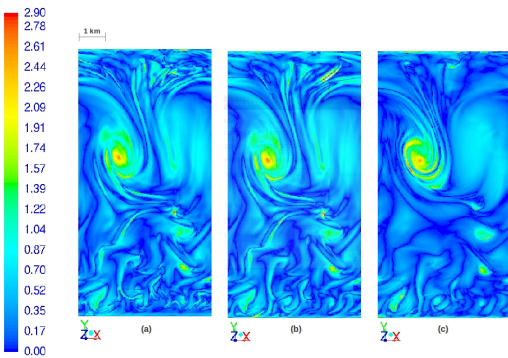


Fig. 9. Rossby number distribution at 25 m depth: (a) RSM, (b) MS and (c) SS.

of the horizontal velocity taken within and below the mixed layer for each of the three modelling approaches. Within and below the mixed layer, due to the highly curved nonlinear flow (Fig. 4). induced by the sub-mesoscale turbulent structures (Fig. 6). and the non-isotropic grid used in the calculations the modelling approach using the RSM model predicts a wave-number spectrum with a different shape than

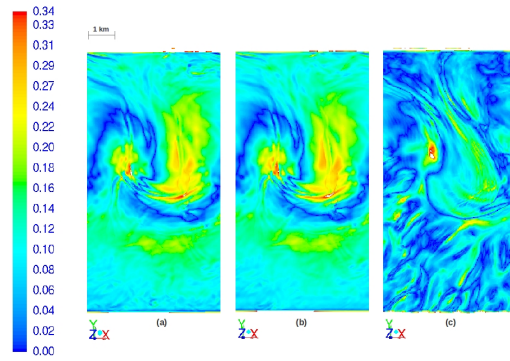


Fig. 10. Rossby number distribution at 75 m depth: (a) RSM, (b) MS and (c) SS.

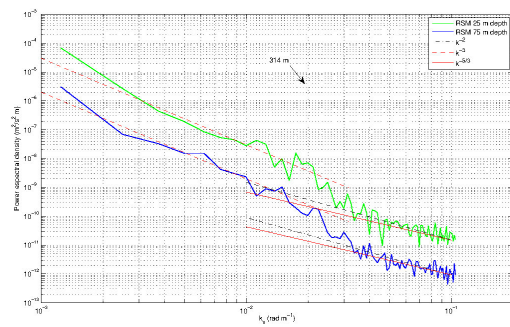


Fig. 11. Wave-number spectra of horizontal velocity URANS-RMS.

those predicted by the modelling approach SS (Fig. 13). The correction implemented in the MS approach to use a non-isotropic grid improves the SS predictions. This improvement is more significant below mixed layer in the absence of flow nonlinearities (Fig. 12). Fig. 11. presents the horizontal velocity wave-number spectra computed with the RSM approach. Within and below the mixed layer, large scale structures exhibit a wave-number spec-

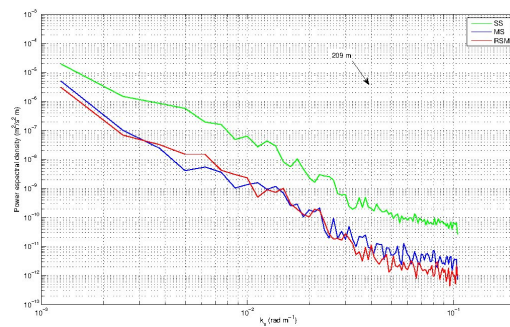


Fig. 12. Wave-number spectra of horizontal velocity: models comparisons below mixing layer.

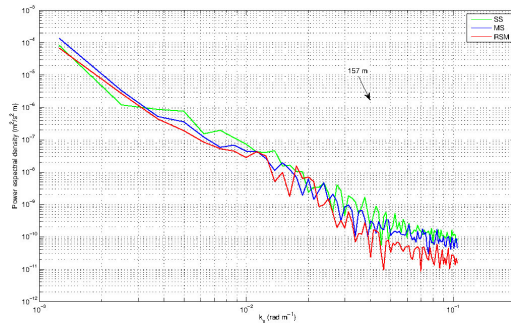


Fig. 13. Wave-number spectra of horizontal velocity: models comparisons within mixing layer.

trum slope of -3 (interior geostrophic theory), whereas the smaller scale structures (< 300 m) present a wave-number spectrum with a slope between -2 (surface quasi-geostrophic theory) and $-5/3$ (surface quasi-geostrophic theory including ageostrophic processes). Given the domain dimensions ($L = 10$ km, $W = 5$ km) and the level of stratification considered in the simulations ($Fr = 0.25$), the flow is forced to a scale that is slightly smaller (2.5 km to 3 km) than the domain width thus prohibiting the development of an inverse energy cascade for the large scale turbulent structures that take place within the mixed layer.

5. DISCUSSION

The frontal system described in the present article has been employed in previous studies. Some of them are shown in Table 1 These studies have focused on describing processes related to sub-mesoscale dynamics, such as the relevance of hydrostatic and non-hydrostatic processes (Mahadevan *et al.* 1996), symmetrical instabilities (Thomas *et al.* 2013), mixing in the ocean surface boundary layer (Skylingstad and Samelson (2012)), changes in the water column stratification induced by sub-mesoscale activity (Mahadevan *et al.* 2010), frontogenesis and stratification in the mixed layer (Özgökmen and Fischer 2012) and its parametrization to capture the restratification process (Fox-Kemper and Ferrari 2008; Kemper *et al.* 2008), among others. Usually, numerical studies focusing on small scale ocean processes use isotropic (Skylingstad and Samelson 2012) or slightly anisotropic grids (Thomas *et al.* 2013; Özgökmen and Fischer 2012), mainly due to the available computing capacity and the number of elements used in the domain discretization. Such studies typically employ linear eddy viscosity turbulence models even

Table 1 Density gradient, Rossby number and vertical velocities in upper ocean fronts.

Reference	$\frac{ \Delta\rho_h }{\times 10^{-5}}$ (kg/m^{-4})	Ro	w $\times 10^{-4}$ (m/s)
Mahadevan <i>et al.</i> (1996)	2.9	-	-3 ~ 1
Skylingstad and Samelson (2008)	1.4	3 ~ 5	-2.4 ~ 0.8
Capet <i>et al.</i> (2008)	12	0.6 ~ 1.2	-7.5 ~ 4.1
Flament <i>et al.</i> (1985)	3	-	-1.1
Paduan and Niiler (1990)	0.3	-	-1.7
Dewey <i>et al.</i> (1991)	0.4 ~ 1	-	-4.6 ~ 4.6
Pollard and Regier (1992)	0.3 ~ 1.3	-	4.6

when the flow fields being described present nonlinearities due to turbulent structures formed as a product of the instabilities developed in the front. According to Launder *et al.* (2006) and Flament *et al.* (2011), such flow fields would not be well described by linear models. On the other hand, in numerical models that involve larger domains sizes (Mahadevan *et al.* 1996; Mahadevan *et al.* 2010), or in studies that describe sub-mesoscale processes using regional oceanographic models (Capet *et al.* 2008; Capet *et al.* 2008), the compromise between computational cost and the admissible grid resolution leads to the independent representation of horizontal and vertical turbulent diffusion. This approach prevents the redistribution of the turbulent kinetic energy contained in the normal velocity fluctuations due to pressure fluctuations (Launder *et al.* 2006; Flament *et al.* 2011). The Reynolds Stress Model does not describe the stress production by weighting the mean velocity gradients isotropically. Instead, it solves an additional conservation equation for each component of the stress tensor, including a production term that is compatible with non-isotropic turbulence, as shown in 11. Although at a higher computational cost, the RSM model allows for a description of the redistribution of the turbulent kinetic energy contained in the normal velocity fluctuations through the pressure strain term. Table 1 summarizes modelling results and field measurements (from Table 1) in Capet *et al.* (2008)) of upper ocean fronts available in the literature in terms of front intensity $\delta\rho_h$, Rossby number and vertical velocity. The front intensity in most cases, including the present study, reached $O(10^{-5})$ kg/m^{-4} , except in Capet *et al.* (2008) and Dewey *et al.* (1991), where it reached a higher value of $O(10^{-4})$ kg/m^{-4} . In all cases $Ro \geq 1$, and the vertical velocities were $O(10^{-4})$ m/s. Below and within the mixed layer, outside of the sub-mesoscale structures, the pre-

dicted vertical velocity magnitude was $O(10^{-4})$ m/s, similar to values obtained in other numerical and experimental studies (Table 1). However, within the mixed layer, the positive (negative) vertical velocities were $O(10^{-3})(O(10^{-2}))$ m/s. These values are higher than those reported elsewhere (Table 1). The asymmetry in the magnitude of both positive and negative vertical velocities coincides with results reported by Mahadevan *et al.* (1996). Some studies of large scale upper ocean front have described submesoscale structures as mesoscale filaments with high Rossby number and high vertical velocity magnitudes (Mahadevan *et al.* 1996; Mahadevan *et al.* 2010) but where non-hydrostatic effects still are difficult to diagnose. In the present work, paying attention to small scale processes, the submesoscale structures were simulated directly. In this case we found some submesoscale filaments where vertical velocity magnitude scales horizontal velocity magnitude and therefore non-hydrostatic effects are relevant (Fig. 7). The non-isotropic grid correction proposed by Rhines (1993) allows for the improved prediction of vertical velocities within the mixed layer. Simulations using the SS model underestimate their magnitude by 50 % with respect to predictions of the nonlinear RSM model and the MS model, which are in accordance with the predictions of the surface quasi-geostrophic theory showed in Ali *et al.* (2009). Under the mixed layer, the predicted vertical velocity magnitude is similar in all three modelling approaches and is consistent with others numerical results and field measurements (Table 1). There are several theoretical descriptions that predict the shape of the horizontal wave-number spectrum. The work by Callies and Ferrari (2013) presents a good summary of these descriptions, explaining how the interior quasi-geostrophic theory, surface quasi-geostrophic theory and surface quasi-geostrophic with ageostrophic modifications predict slopes of -3 , -2 and $-5/3$, respectively. In the same work, Callies and Ferrari (2013) shows predictions of wave-number spectra for cases considering constant and exponential stratification, where the slope of the spectra associated with scales smaller than 3 km fits $k^{-5/3}$ and coincides with our predicted results within and below mixed layer for scales smaller than 150 m. For the simulated conditions considered in the present article, the Froude number is estimated according to Skillingstad and Samelson (2008): $Fr = U/NH = Ri_d^{-1/2}$, with $Ri_d = N^2 H^2 U^2$ the bulk Richardson number and U the horizontal velocity scale. We obtained a value of $Fr = 0.25$. The study by Özgökmen

et al. (2011) reported the characteristics of mixed layer sub-mesoscale structures in numerical simulations considering two stratification conditions: $Fr=0.1$ and $Fr=1$. We found similar results to those reported by Özgökmen *et al.* (2011) for $Fr = 0.1$, where the evolution of the front instabilities generated a moderate amount of sub-mesoscale structures with length scales of ≈ 2 km, which remained confined close to the surface. We did not observe the flow characteristics present in the simulation of $Fr = 1$, that is, a high number of smaller scale turbulent structures < 500 m, with a deeper penetration. In addition, the shape of the horizontal spectrum for the wave numbers between $k = 10^{-3}$ and $k = 10^{-2}$ predicted in our simulations within the mixing layer is in agreement with Özgökmen *et al.* (2011) for $Fr=0.1$, reaching, for the same range of k , a slope of -3 instead of the slope of $-5/3$ reported by Özgökmen *et al.* (2011) for $Fr=1$.

6. SUMMARY AND CONCLUSIONS

By introducing trivial modifications to the conservation equations of the CFD code ANSYS-FLUENT, we included the effects of the Earth's rotation and water column stratification and implemented a high-resolution, non-hydrostatic model describing the submesoscale dynamics in a small scale (10 km) mid-latitude upper ocean front. Through the simulation of the periodic system, we studied the small-scale turbulent characteristics present in upper ocean frontal systems. This allowed us to directly calculate the submesoscale structures generated in the front, finding positive (negative) vertical velocities one (two) order(s) of magnitude higher than those associated with sub-mesoscale ($O(10^{-4})$ m/s) processes reported in previous numerical and experimental studies. To describe subgrid-scale turbulent structures three different approaches were used:

- Standard Smagorinsky model: a linear eddy viscosity model where the turbulent viscosity is estimated using an algebraic equation.
- Modified Smagorinsky model, which includes a modification to the standard version to correct the calculation of the turbulent viscosity when non-isotropic computational grids are used.
- Reynolds stress model, which describes each one of the components of the Reynolds stress tensor through the solution of an additional conservation equation.

Results from the RSM and MS approaches predict a mixed layer with the following characteristics: high vertical velocity magnitudes that scale with predictions from surface quasi-geostrophic theory, a high curvature nonlinear flow field, and ($Ro > 1$). These characteristics are attributable to the existence of submesoscale turbulent structures confined within the first 50 m depth. Under the mixed layer, the results show a low vertical velocity that is one order of magnitude lower than that found within the mixed layer, $Ro < 0.4$, and a low curvature linear flow field. Within and below the mixed layer the horizontal wave-number spectra predicted with the RSM approach differs from the spectra predicted with SS approach. The correction implemented in the MS approach to use a non-isotropic grid improves the SS predictions on both the flow structure and spectral energy distributions. This improvement is more significant below mixed layer in the absence of flow nonlinearities. However, within the mixed layer due to the highly curved flow the differences still persist among RSM and MS predictions especially for the smaller scales. This work contributes to the investigation of the physical and methodological aspects for the detailed modelling and understanding of small scale structures in ocean turbulence.

7. PERSPECTIVES

The continuation of this work involves the study of the forward and inverse energy flux for extreme values of $\frac{N}{f}$ in the context of an upper ocean front using a non-hydrostatic LES model and the modified version of the Smagorinsky subgrid-scale model.

ACKNOWLEDGMENTS

PC was funded by the CONICYT program for doctoral studies en Chile, the Mechanical Engineering Department of the University of Concepcion and the CONICYT/FONDAP Project-15130015. HHS was hosted at the Laboratoire de Physique des Océans, Université de Bretagne Occidentale, Brest, France, under the University of Concepcion Fellowship, while finishing this manuscript. Computing resources were provided by the Geophysics Department (DGEO) and Mechanical Engineering Department (DIM), University of Concepción.

REFERENCES

Allmaras, S. and Spalart, P. (1992). A one-equation turbulence model for aerodynamic flows. *Technical Report AIAA-92-0439*. American Institute of Aeronautics

and Astronautics

- Aman, F., A. Ishak and I. Pop (2008 January). Parameterization of Mixed Layer Eddies. Part I: Theory and Diagnosis. *Journal of Physical Oceanography* 38(6), 1145–1165.
- Blumen, W. (1978). Uniform Potential Vorticity Flow: Part I. Theory of Wave Interactions and Two-Dimensional Turbulence. *Journal of the Atmospheric Sciences* 35(5), 774–783.
- Boffetta, G., Celani, A. and Vergassola, M. (2000). Inverse energy cascade in two-dimensional turbulence : Deviations from Gaussian behavior. *Physica Review E* 61(1), 29–32.
- Boccaletti, G., R. Ferrari and B. Fox-Kemper (2007, September). Mixed Layer Instabilities and Restratification. *Journal of Physical Oceanography* 37(9), 2228–2250.
- Boyd, J. P. (1992). The Energy Spectrum of Fronts: Time Evolution of Shocks in Burgers Equation. *Journal of the Atmospheric Sciences* 49(2), 128–139.
- Callies, J. and R. Ferrari (2013 November). Interpreting Energy and Tracer Spectra of Upper-Ocean Turbulence in the Submesoscale Range (1200 km). *Journal of Physical Oceanography* 43(11), 2456–2474.
- Capet, X., J. C. McWilliams, M. J. Molemaker and a. F. Shchepetkin (2008). Mesoscale to Submesoscale Transition in the California Current System. Part III: Energy Balance and Flux. *Journal of Physical Oceanography* 38(10), 2256–2269.
- Capet, X., J. C. McWilliams, M. J. Molemaker and a. F. Shchepetkin (2008). Mesoscale to Submesoscale Transition in the California Current System. Part II: Frontal Processes. *Journal of Physical Oceanography* 38(1), 44–64.
- Capet, X., J. C. McWilliams, M. J. Molemaker and a. F. Shchepetkin (2008 January). Mesoscale to Submesoscale Transition in the California Current System. Part I: Flow Structure, Eddy Flux, and Observational Tests. *Journal of Physical Oceanography* 38(1), 29–43.
- Charney, J. G. (1971). Geostrophic Turbulence. *Journal of the Atmospheric Sciences* 28(6), 1087–1095.

- Charney, J. G. (2011 April). Geostrophic Turbulence. *Science (New York, N.Y.)* 332(6027), 318–22.
- Dewey, R. K., J. N. Moum, C. A. Paulson, D. R. Caldwell and S. D. Pierce (2011 April). Structure and dynamics of a coastal filament. *J. Geophys. Res.* 96, 14885–14907.
- Flament, P., L. Armi and L. Washburn (1985). The evolving structure of an upwelling filament. *J. Geophys. Res.* 90, 11765–11778.
- Fox-Kemper, B. and R. Ferrari (2008). Parameterization of Mixed Layer Eddies. Part II: Prognosis and Impact. *Journal of Physical Oceanography* 38(6), 1166–1179.
- Hanjalić, K. and Launder, B. (2011). *Modelling turbulence in engineering and the environment. Second-moment routes to closure*. Cambridge University Press.
- Jiménez, J. (2010 January). The Contributions of A. N. Kolmogorov to the theory of turbulence. *Arbor CLXXVIII(704)*, 589–606.
- Klein, P., B. L. Hua, G. Lapeyre, X. Capet, S. Le Gentil and H. Sasaki (2008). Upper Ocean Turbulence from High-Resolution 3D Simulations. *Journal of Physical Oceanography* 38(8), 1748–1763.
- Klein, P. and G. Lapeyre (2009 January). The oceanic vertical pump induced by mesoscale and submesoscale turbulence. *Annual review of marine science* 2013(1), 351–75.
- Klein, P., G. Lapeyre, G. Roulet, S. Le Gentil and H. Sasaki (2011). Ocean turbulence at meso and submesoscales: connection between surface and interior dynamics. *Geophysical & Astrophysical Fluid Dynamics* 4-5(105), 421–437.
- Lapeyre, G., P. Klein, and B. L. Hua (2006, August). Oceanic Restratification Forced by Surface Frontogenesis. *Journal of Physical Oceanography* 36(8), 1577–1590.
- Launder, B. E., G. J. Reece and W. Rodi (1975). Progress in the development of a Reynolds-stress turbulence closure. *Journal of Fluid Mechanics* 68(3), 537–566.
- Launder, B. E. (1989). Second-moment closure and its use in modelling turbulent industrial flows. *International Journal for Numerical Methods in Fluids* 9(8), 963–985.
- Launder, B. E., G. J. Reece and W. Rodi (2006 March). Progress in the development of a Reynolds-stress turbulence closure. *Journal of Fluid Mechanics* 68(3), 537.
- Lilly D. K. (1967). The representation of small-scale turbulence in numerical simulation experiments. *Proceedings of the IBM Scientific Computing Symposium on Environmental Science* 28(6), 195.
- Mahadevan, A., A. Tandon and R. Ferrari (2010). Rapid changes in mixed layer stratification driven by submesoscale instabilities and winds. *Journal of Geophysical Research* 115(C3), C03017.
- Mahadevan, A. (2006). Modeling vertical motion at ocean fronts : Are nonhydrostatic effects relevant at submesoscales. *Ocean Modelling* 14, 222–240.
- Mahadevan, A., J. Oliger and Street, R. (1996). A nonhydrostatic mesoscale ocean model. Part II: Numerical implementation. *Journal of Physical Oceanography* 26, 1881–1900.
- Martin, A. P. and K. J. Richards (2001 January). Mechanisms for vertical nutrient transport within a North Atlantic mesoscale eddy. *Deep Sea Research Part II: Topical Studies in Oceanography* 484-5, 757–773.
- McWilliams, J. C. (2008). Fluid dynamics at the margin of rotational control. *Environmental Fluid Mechanics* 85-6, 441–449.
- Molemaker, M. J., J. C. McWilliams and X. Capet (2010 January). Balanced and unbalanced routes to dissipation in an equilibrated Eady flow. *Journal of Fluid Mechanics* 654, 35–63.
- Molemaker, M. J. and J. C. McWilliams (2005). Baroclinic Instability and Loss of Balance. *Journal of Physical Oceanography* 35, 1505–1517.
- Müller, P. (2005). Routes to dissipation in the ocean: The 2D/3D turbulence conundrum. *Marine turbulence: theories ...* 654, 35–63.
- Özgökmen, T. M. and P. F. Fischer (2012 July). CFD application to oceanic mixed layer sampling with Lagrangian platforms. *International Journal of Computational Fluid Dynamics* 26(6-8), 337–348.

- Özgökmen, T. M., A. C. Poje, P. F. Fischer and A. C. Haza (2011 January). Large eddy simulations of mixed layer instabilities and sampling strategies. *Ocean Modelling* 39(3-4), 311–331.
- Paduan, J. and Niiler, P. (1990). A Lagrangian description of motion in northern California coastal transition filaments. *J. Geophys. Res.* 95, 18095–18109.
- Perot, B. (1999). Turbulence modeling using body force potentials. *Physics of Fluids (1994-present)*. 11, 609–624.
- Pollard, R. and Regier, L. (1992). Vorticity and vertical circulation at an ocean front. *J. Phys. Oceanogr.* 22, 609–624.
- Ramachandran, S., A. Tandon and A. Mahadevan (2013). Effect of subgrid-scale mixing on the evolution of forced submesoscale instabilities. *Ocean Modelling*. 66, 45–63.
- Rhines, P. B. (1979). Geostrophic Turbulence. *Annu. Rev. Fluid Mech.* 11, 401–441.
- Rhines, P. B. (2006 Mar). Waves and turbulence on a beta-plane. *Journal of Fluid Mechanics* 69(3), 417.
- Scotti, A., C. Meneveau, D. K. Lilly and K. Douglas (1993 September). Generalized Smagorinsky model for anisotropic grids. *Physics of Fluids A: Fluid Dynamics* 5(9), 2306–2308.
- Smagorinsky, J. (1963). General Circulation Experiments with the Primitive Equations. I. The Basic Experiment. *Monthly weather review* 91(3), 99–164.
- Skyllingstad, E. D. and Samelson, R. M. (2012 October). Baroclinic Frontal Instabilities and Turbulent Mixing in the Surface Boundary Layer. Part I: Unforced Simulations. *Journal of Physical Oceanography* 42(10), 1701–1716.
- Thomas, L. N., A. Tandon and A. Mahadevan (2008). Submesoscale Processes and Dynamics. *Ocean Modeling in an Eddy Regime* 42(10), 1701–1716.
- Thomas, L. N., J. R. Taylor, R. Ferrari and T. M. Joyce (2013 July). Symmetric instability in the Gulf Stream. *Deep Sea Research Part II: Topical Studies in Oceanography* 91(10), 96–110.
- Van Roekel, L. P., P. E. Hamlington and B. Fox-Kemper (2012). Multiscale simulations of Langmuir cells and submesoscale eddies using XSEDE resources. *Proceedings of the 1st Conference of the Extreme Science and Engineering Discovery Environment on Bridging from the eXtreme to the campus and beyond - XSEDE '12* 1.
- Wunsch, C. and Ferrari, R. (2004 January). Vertical Mixing, Energy, and the General Circulation of the Oceans. *Annual Review of Fluid Mechanics* 36(1), 281–314.